24th INTERNATIONAL CONGRESS ON SOUND AND VIBRATION
23–27 July 2017, London

# ANALYSIS AND IMPLEMENTATION OF A MULTIPLE-SOURCE MULTIPLE-CHANNEL ACTIVE VIBRATION CONTROL OF LARGE STRUCTURES BASED ON FINITE ELEMENT MODEL IN-LOOP SIMULATION SYSTEM

Jinxin Liu, Xingwu Zhang, Liangdong Yang and Xuefeng Chen

*Xi'an Jiaotong University, State Key Laboratory for Manufacturing Systems Engineering, Xi'an, China*
*email: Jinxin.liu@xjtu.edu.cn*

Bei Gao

*Xi'an Jiaotong University, the National Demonstration Centre of Experimental Teaching, School of Mechanical Engineering, Xi'an, China*

In the active vibration control of large structures, multiple-channel, i.e., multiple-input and multiple-output (MIMO), control is required, since there are usually multiple vibration sources, the force of actuators are limited and the control objective is usually global. Resulting from the complex dynamic behaviour of large structures, the performance of MIMO control will be dramatically influenced. Thus, the design of controller should base on the structural analysis of the controlled plant. However, the present structural analysis methods for large structure (e.g., finite element method) are separated from the controller design and simulation process. In this paper, we embed the finite element model into the control loop to form a finite element model in-loop simulation (FEMilS) scheme for active vibration control. First, we extend the active noise equalization (ANE) algorithm, a universal narrowband adaptive control algorithm, to MIMO, so that it is able to cope with large structures. Then, the convergence analysis of the MIMO-ANE algorithm is conducted. Afterward, the FEMilS scheme is systematically illustrated. Finally, MIMO-ANE control case studies that considering multiple primary sources are conducted on a variable section cylindrical structure based on FEMilS. The simulations have similar procedure to real-life control and can be easily extended to physical model platform.
Keywords: Active Vibration Control, MIMO, Narrowband

## 1. Introduction

In the active vibration control (AVC) of large structures, multiple-channel, i.e., multiple-input multiple-output (MIMO), control is required, since there are usually multiple vibration sources, the force of actuators are limited and the control objectives are usually global. Most of the vibrations are caused by rotational machines (e.g., engines, propellers, compressors and motors), producing line-spectral vibrations [1, 2]. The line-spectral vibration will reduce structural strength and ride comfort of vehicles and, specially, reduce detection ability and stealth of military vehicles. Narrowband active vibration control algorithm is specialized for the control of line-spectral vibrations [3]. There are lots of methods, like optimal control, pole placement, robust method, adaptive method, positive position feed-back (PPF), etc., for controller design, in which the adaptive method is the focus of interest due to its self-adaption capability [4]. The most popular adaptive method for active control is called filtered-reference LMS (FXLMS) algorithm, in which the narrowband FXLMS is very popular in multiple-source and multiple-harmonic control application [5]. Active noise equalization (ANE) algorithm is one of the most general narrowband FXLMS algorithms, which can can-

cel, supress, neural and enhance the line-spectral vibration [6, 7]. Thus, it provided a universal solution to line-spectral vibration control, no matter cancelling or reshaping.

In the active control system, an analytical model can act as a controlled plant if it is simple. However, for a complex plant, the analytical model is difficult or even impossible to obtain. Fortunately, with the development of computer technology, finite element model has been introduced as the controlled plant for the controller design and verification. Some researchers integrated the control algorithm into the CAE software [8]. Some other researchers extracted the state space model from the FE model [9] or directly solved the dynamic response of the FE model [10], and then conducted the control on the extracted numerical model.

In this paper, we will conduct a multiple-source and multiple-channel active vibration control on the finite element model of a variable section cylindrical structure. First, we will extend the active noise equalization (ANE) algorithm to MIMO, so that it is able to cope with large structures. Then, the convergence analysis of the MIMO-ANE algorithm is conducted. Afterward, a finite element model in-loop simulation (FEMilS) scheme is systematically illustrated. Finally, two case studies of 2-soruce-2-input-2-output active vibration control were conducted based on FEMilS.

## 2. Universal MIMO Narrowband FXLMS Algorithm

Narrowband FXLMS algorithm is specialized for the line-spectral vibration control. ANE algorithm is a universal narrowband FXLMS algorithm which is able to cancel, supress, neutral and enhance the primary noise and vibration. Next, we will extend ANE to MIMO using matrix representation.

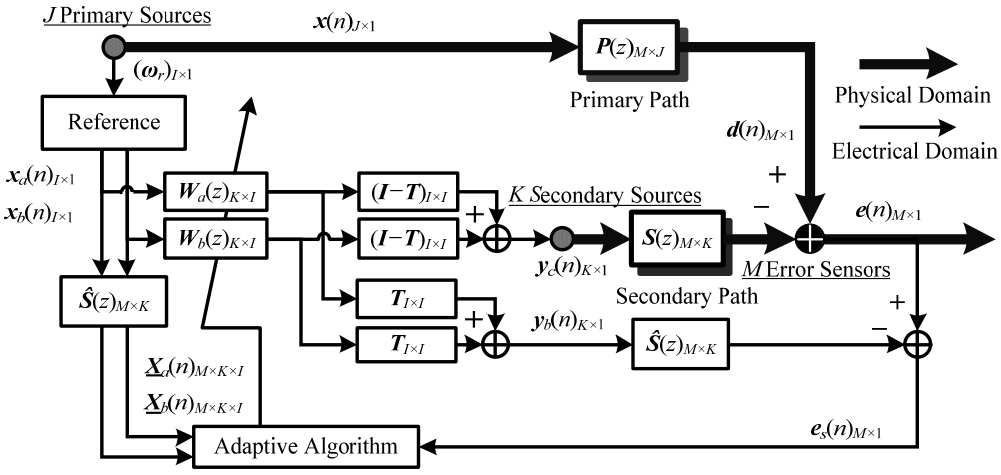


Figure 1: diagram of MIMO-ANE system

As shown in Figure **1**, we consider *J* primary sources, *K* secondary sources and *M* error sensors, in which the $i^{\text{th}}$ primary source contains $I_j$ frequency component. For narrowband FXLMS algorithm, all the frequencies of all the sources can be combined into one (*I*×1) dimensional column vector to generate reference signals, i.e.,

$$\boldsymbol{\omega}_r = \{\omega_{ri}\}^T, \quad i = 1, 2, ..., I, \tag{1}$$

where $I = \sum_{j=1}^{J} I_j$. Accordingly, two (*I*×1) dimensional reference vectors can be defined as

$$\boldsymbol{x}_a(n) = \{x_{ai}(n)\}^T = \cos\boldsymbol{\omega}_r, \ \boldsymbol{x}_b(n) = \{x_{bi}(n)\}^T = \sin\boldsymbol{\omega}_r, \ i = 1, 2, ..., I. \tag{2}$$

For each secondary source and each frequency component there will be two coefficients in the controller. Thus, the controller coefficients can be defined as two (*K*×*I*) dimensional matrixes, i.e.,

$$\boldsymbol{W}_a(n)=\left[w_{aki}(n)\right],\ \boldsymbol{W}_b(n)=\left[w_{bki}(n)\right],\ k=1,2,...,K,\ i=1,2,...,I\,, \tag{3}$$

where $w_{aki}(n)$ and $w_{bki}(n)$ denotes the controller coefficients for the $k^{\text{th}}$ secondary source and the $i^{\text{th}}$ frequency component. ANE system makes use of equalization parameters for the residual spectrum reshaping. The equalization parameters can be defined as a ($I$×$I$) dimensional diagonal matrix, i.e.,

$$\boldsymbol{T}=\mathrm{diag}\left\{\beta_i\right\},\ i=1,2,...,I\,, \tag{4}$$

where $\beta_i$ denotes the equalization parameter of the $i^{\text{th}}$ frequency component. ANE system has two branches, in which one, called cancelling branch, is used to drive the secondary sources and the other, called equalization branch, is used to build pseudo-error signal. According to Eqs.(2)-(4), the output of the cancelling and equalization branch ANE can be expressed as

$$\boldsymbol{y}_c(n)=\boldsymbol{W}_a(n)\left(\boldsymbol{I}-\boldsymbol{T}\right)\boldsymbol{x}_a(n)+\boldsymbol{W}_b(n)\left(\boldsymbol{I}-\boldsymbol{T}\right)\boldsymbol{x}_b(n)\,, \tag{5}$$

$$\boldsymbol{y}_b(n)=\boldsymbol{W}_a(n)\boldsymbol{T}\boldsymbol{x}_a(n)+\boldsymbol{W}_b(n)\boldsymbol{T}\boldsymbol{x}_b(n)\,, \tag{6}$$

where $\boldsymbol{y}_c(n)$ and $\boldsymbol{y}_b(n)$ are both ($K$×1) dimensional vectors. The real-error signals are superposition of primary noises and secondary noises, i.e.,

$$\boldsymbol{e}(n)=\boldsymbol{d}(n)-\boldsymbol{S}(n)*\boldsymbol{y}_c(n)\,, \tag{7}$$

where $\boldsymbol{e}(n)$ denotes ($M$×1) dimensional real-error vector, $\boldsymbol{d}(n)$ denotes ($M$×1) dimensional primary noise vector, $\boldsymbol{S}(n)$ denotes ($M$×$K$) dimensional impulse response function matrix of secondary path, in which the element $s_{mk}(n)$ denotes the impulse response function from the $k^{\text{th}}$ secondary source to the $m^{\text{th}}$ error sensor, and * denotes linear convolution. The pseudo-error vector is used to feedback to the adaptive algorithm for the controller coefficients updating. It can be express as a ($M$×1) dimensional vector, i.e.,

$$\boldsymbol{e}_s(n)=\boldsymbol{e}(n)-\hat{\boldsymbol{S}}(n)*\boldsymbol{y}_b(n)\,, \tag{8}$$

where $\hat{\boldsymbol{S}}(n)$ is the identification of $\boldsymbol{S}(n)$. The filtered reference signals are also required for the controller coefficients updating. They are ($M$×$K$×$I$) dimensional matrixes, i.e.,

$$\underline{\mathbf{X}}'_a(n)=\hat{\boldsymbol{S}}(n)*\boldsymbol{x}_a(n),\ \underline{\mathbf{X}}'_b(n)=\hat{\boldsymbol{S}}(n)*\boldsymbol{x}_b(n)\,, \tag{9}$$

According to the stochastic descent method, the updating equation of the controller coefficient can be expressed as

$$\boldsymbol{W}_l(n+1)=\boldsymbol{W}_l(n)+\mu_l\underline{\mathbf{X}}'^{T}_l(n)\boldsymbol{e}_s(n),\ l=a,b\,, \tag{10}$$

where $\underline{\mathbf{X}}'^{T}_l$ is transpose of $\underline{\mathbf{X}}'_l$ and is a ($K$×$I$×$M$) dimensional matrixes.

## 3. Convergence Boundary

Due to the coupling between multiple secondary sources and multiple error sensors, the convergence of the MIMO-ANE system will be dramatically affected by the characteristics of the eigenvalue of the FRF matrix. The influence of secondary path to different frequency component is different. For the $i^{\text{th}}$ frequency component, the secondary path matrix will introduce amplitude ratios and phase differences, which can be defined as ($M$×$K$) dimensional matrixes, i.e.,

$$\boldsymbol{P}_{si}=\left[\left|s_{mk}(j\omega_i)\right|\right],\boldsymbol{\Phi}_{si}=\left[\angle s_{mk}(j\omega_i)\right],m=1,2,...,M,k=1,2,...,K\,. \tag{11}$$

From Eqs.(5)-(8), consider $\hat{\boldsymbol{S}}(n)=\boldsymbol{S}(n)$, and expand the controller coefficients and reference signal, there is

$$\boldsymbol{e}_s(n)=\boldsymbol{d}(n)-\boldsymbol{S}(n)*\sum_{i=1}^{I}\left[\boldsymbol{w}_{ai}(n)x_{ai}(n)+\boldsymbol{w}_{ai}(n)x_{ai}(n)\right]. \tag{12}$$

Exchange the position of controller coefficient and secondary path matrix, there is

$$\boldsymbol{e}_s(n)=\boldsymbol{d}(n)-\sum_{i=1}^{I}\boldsymbol{w}_{ai}(n)\left[\boldsymbol{S}(n)*x_{ai}(n)\right]-\sum_{i=1}^{I}\boldsymbol{w}_{bi}(n)\left[\boldsymbol{S}(n)*x_{bi}(n)\right]. \tag{13}$$

According to Eq.(11), the filtered reference of $i^{\text{th}}$ component can be expressed as

$$\begin{aligned}\boldsymbol{X}'_{ai}(n)&=\boldsymbol{S}(n)*x_{ai}(n)=\boldsymbol{P}_{si}\left[\cos\boldsymbol{\Phi}_{si}\cdot x_{ai}(n)-\sin\boldsymbol{\Phi}_{si}\cdot x_{bi}(n)\right],\\ \boldsymbol{X}'_{bi}(n)&=\boldsymbol{S}(n)*x_{bi}(n)=\boldsymbol{P}_{si}\left[\sin\boldsymbol{\Phi}_{si}\cdot x_{ai}(n)+\cos\boldsymbol{\Phi}_{si}\cdot x_{bi}(n)\right],\end{aligned} \tag{14}$$

where $\cos\boldsymbol{\Phi}_{si}$ and $\sin\boldsymbol{\Phi}_{si}$ are defined as $\left[\cos\phi_{mki}\right]$ and $\left[\sin\phi_{mki}\right]$, respectively, for all $m$ = 1,2,…$M$, $k$ = 1,2,…,$K$. Substitute Eq.(14) into Eq.(13), the pseudo-error vector can be written as

$$\boldsymbol{e}_s(n)=\boldsymbol{d}(n)-\sum_{i=1}^{I}\left[\boldsymbol{w}'_{ai}(n)x_{ai}(n)+\boldsymbol{w}'_{bi}(n)x_{bi}(n)\right]. \tag{15}$$

where

$$\boldsymbol{w}'_{ai}(n)=\boldsymbol{P}_{si}\left[\cos\boldsymbol{\Phi}_{si}\cdot\boldsymbol{w}_{ai}(n)+\sin\boldsymbol{\Phi}_{si}\cdot\boldsymbol{w}_{bi}(n)\right],\ \boldsymbol{w}'_{bi}(n)=\boldsymbol{P}_{si}\left[\cos\boldsymbol{\Phi}_{si}\cdot\boldsymbol{w}_{bi}(n)-\sin\boldsymbol{\Phi}_{si}\cdot\boldsymbol{w}_{ai}(n)\right]. \tag{16}$$

Suppose the primary noises $\boldsymbol{d}(n)$ are defined as

$$\boldsymbol{d}(n)=\sum_{i=1}^{I}\left[\boldsymbol{a}_i x_{ai}(n)+\boldsymbol{b}_i x_{bi}(n)\right], \tag{17}$$

where $\boldsymbol{a}_i$ and $\boldsymbol{b}_i$ are both ($M$×1) dimensional coefficients vectors for primary noises. According to Eqs.(15)-(17), the expectation of the squared pseudo-error can be expressed as

$$E\left[\boldsymbol{e}_s^T(n)\boldsymbol{e}_s(n)\right]=\sum_{i=1}^{I}\left[\boldsymbol{c}_i-\boldsymbol{S}_i\boldsymbol{w}_i(n)\right]^T\left[\boldsymbol{c}_i-\boldsymbol{S}_i\boldsymbol{w}_i(n)\right], \tag{18}$$

where

$$\boldsymbol{c}_i=\begin{bmatrix}\boldsymbol{a}_i\\ \boldsymbol{b}_i\end{bmatrix},\ \boldsymbol{w}_i(n)=\begin{bmatrix}\boldsymbol{w}_{ai}(n)\\ \boldsymbol{w}_{bi}(n)\end{bmatrix},\ \boldsymbol{S}_i=\begin{bmatrix}\boldsymbol{P}_{si}\cos\boldsymbol{\Phi}_{si} & \boldsymbol{P}_{si}\sin\boldsymbol{\Phi}_{si}\\ -\boldsymbol{P}_{si}\sin\boldsymbol{\Phi}_{si} & \boldsymbol{P}_{si}\cos\boldsymbol{\Phi}_{si}\end{bmatrix}. \tag{19}$$

The gradient to the $i^{\text{th}}$ controller coefficient vector is

$$\frac{\partial E\left[\boldsymbol{e}_s^T(n)\boldsymbol{e}_s(n)\right]}{\partial\boldsymbol{w}_i(n)}=-2\boldsymbol{S}_i^T\left[\boldsymbol{c}_i-\boldsymbol{S}_i\boldsymbol{w}_i(n)\right]. \tag{20}$$

The update equation of the $i^{\text{th}}$ controller coefficient in mean square sense (using upper bar) can be express as

$$\bar{\boldsymbol{w}}_i(n+1)=\left[\boldsymbol{I}-\mu_i\boldsymbol{S}_i^T\boldsymbol{S}_i\right]\bar{\boldsymbol{w}}_i(n)+\mu_i\boldsymbol{S}_i^T\boldsymbol{c}_i. \tag{21}$$

Let

$$\bar{\boldsymbol{v}}_i(n)=\bar{\boldsymbol{w}}_i(n)-(\boldsymbol{S}_i^T\boldsymbol{S}_i)^{-1}\boldsymbol{S}_i^T\boldsymbol{c}_i. \tag{22}$$

There is

$$\bar{\boldsymbol{v}}_i(n+1)=\left[\boldsymbol{I}-\mu_i\boldsymbol{S}_i^T\boldsymbol{S}_i\right]\bar{\boldsymbol{v}}_i(n). \tag{23}$$

The auto-correlation matrix of secondary path is a ($K\times K$) dimensional matrix and can be decomposed as

$$\boldsymbol{S}_i^T\boldsymbol{S}_i=\boldsymbol{Q}_i\boldsymbol{\Lambda}_i\boldsymbol{Q}_i^T=\begin{bmatrix}\boldsymbol{P}_{si}^2 & 0\\ 0 & \boldsymbol{P}_{si}^2\end{bmatrix}, \tag{24}$$

where $\boldsymbol{Q}_i$ is the modal matrix, and $\boldsymbol{\Lambda}_i=\mathrm{diag}\left[\lambda_{ki}\right]$ is the eigenvalue matrix. Since $\boldsymbol{S}_i^T\boldsymbol{S}_i$ is nonnegative definite, $\lambda_{ki}\geq 0$ for all $i$ = 1,2,…,$I$. Define the rotation vector as

$$\bar{\boldsymbol{v}}_i^R(n)=\boldsymbol{Q}_i^T\bar{\boldsymbol{v}}_i(n). \tag{25}$$

There is

$$\bar{\boldsymbol{v}}_i^R(n+1)=\left[\boldsymbol{I}-\mu_i\boldsymbol{\Lambda}_i\right]\bar{\boldsymbol{v}}_i^R(n). \tag{26}$$

For the $i^{\text{th}}$ frequency component, the system convergence when

$$\left|1-\mu_i\lambda_{ki}\right|<1, \text{ for all } k = 1,2,\ldots,K. \tag{27}$$

Thus the boundary of the step-size is

$$0<\mu_i<\frac{2}{\rho_i}=\frac{2}{\max\limits_{1\leq k\leq K}\lambda_{ki}}, \tag{28}$$

where $\rho_i$ is spectral radius of $\boldsymbol{S}_i^T\boldsymbol{S}_i$ .From Eq.(24), it can be seen that the convergence of the $i^{\text{th}}$ frequency component of MIMO-ANE are influenced by the amplitude ratio of secondary transfer matrix at the $i^{\text{th}}$ frequency. More specifically, from Eq.(28) the maximum step-size of $i^{\text{th}}$ frequency component is restricted by the spectral radius, i.e., the maximum eigenvalue of $\boldsymbol{S}_i^T\boldsymbol{S}_i$ . The larger the spectral radius is, the smaller the upper bound of step-size will be.

## 4. Finite Element Model in-loop Simulation System

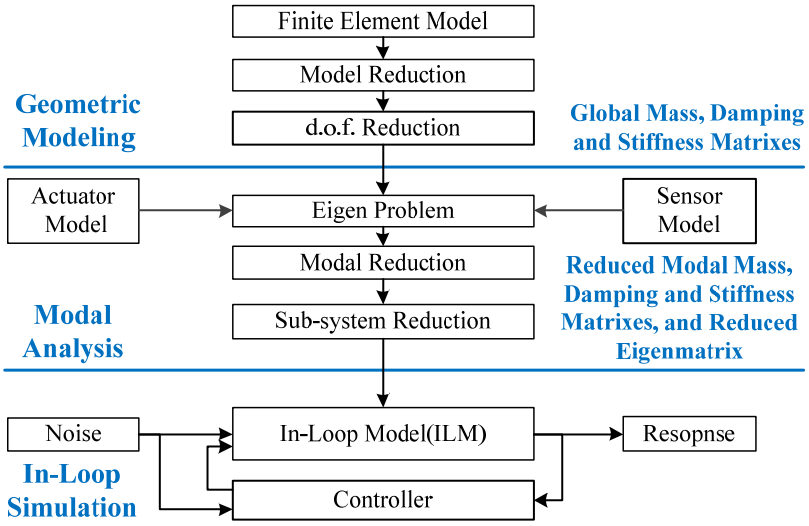


Figure 2: Procedure of FEMilS

The basic idea of finite element model in-loop simulation system (FEMilS) is to design the controller based on the dynamic of the controlled plant. The FEMilS is achieved by embed the finite element model into the AVC simulation loop, so it is a time domain point-by-point simulation whose procedure and structure are similar to that of real-life control. The general procedure of

FEMilS is shown in Figure **2**. It can be divided into three stages, i.e., geometric modelling, modal analysis and in-loop simulation. In the geometric modelling stage, a simplified model can be first obtained by geometrical simplification and degree of freedom (DOF) reduction. Then the global mass matrix, global stiffness matrix and/or global damping matrix are extracted. In the modal analysis stage, the model can be further reduced by modal reduction and sub-system reduction. Then the reduced modal mass matrix, reduced modal stiffness matrix, reduced modal damping matrix and reduced eigenmatrix are obtained. In the in-loop simulation stage, an in-loop model (ILM) for simulation is first constructed according to the above reduced matrixes. Then the dynamic response analysis and AVC are conducted. The first two stages can be viewed as pre-processing which prepares the ILM for simulation. The third stage is the finally simulation stage. The details of the three stages that presented based on a variable section cylinder can be found in reference [2].

## 5. Control Simulation

### 5.1 The Finite Element model

As shown in Figure **3**, the finite element model for FEMilS is a variable section cylindrical structure, which may have application in many mechanical structures, such as rockets, submarines, airplanes and trains. The cylinder is divided into 20×16 rectangle elements and the baffle is divided into 16 quadrilateral elements. Each element has four nodes and adjacent elements share two nodes, so there are 356 nodes in total. Each node has six DOFs, so the total DOFs are 2136 (356×6) if the cylinder is unconstrained. The translations along *xyz* axis are considered to be main DOFs of the system, thus reducing the total DOFs to be 1068 (356×3). The mass and stiffness matrix are extracted from ANSYS by super element method and outputted in Harwell-Boeing format (sparse). The size of those matrixes is 1068×1068. A few low-order modes are usually dominating, so the computational speed improvement by modal reduction is significant. We consider the first 16 low-order mode in this case. As illustrated in Figure **3**, if we only consider the four points (P1-P2), a (4×4) subsystem can be further extracted from the finite element model, which can further reduce the computational complexity. As a consequence, we obtained the ILM for simulation.

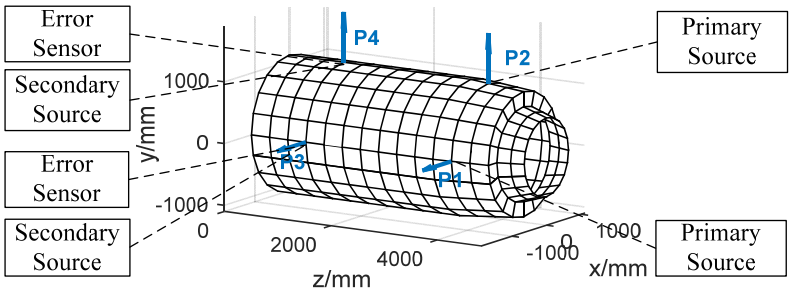


Figure 3: FE model of a variable section cylindrical structure for FEMilS

### 5.2 Case A: 2-source-2-input-2-output active vibration cancelation

In case A, primary sources are supposed to be placed at P1 and P2, secondary sources and error sensors are supposed to be placed at P3 and P4. The primary forces are shown in Figure **4** (a) and (b). P1 contains 10Hz, 20Hz, 30Hz, 40Hz and 50Hz component with amplitude of 1N, 2N, 5N, 10N and 2N, respectively, with the addition to 20% white noise. P2 contains 15Hz, 45Hz and 75Hz component with amplitude of 3N, 10N and 8N, respectively, with the addition to 20% white noise. The equalization parameter for each component is 0 (i.e., cancellation mode). The sampling frequency is 2048Hz, the sampling time is 6s, and the step-size is $2\times10^{8}$. Figure **4** (c) and (d) shows the real-error signal of P3 and P4. It can be seen that the harmonic can be successfully cancelled and it remains only broadband noises. Figure **4** (e)(f) and (g)(h) shows the controller coefficients of P3 and P4. It can be seen that different frequency component has different convergence rate, which results from the feature of secondary path transfer function matrix.

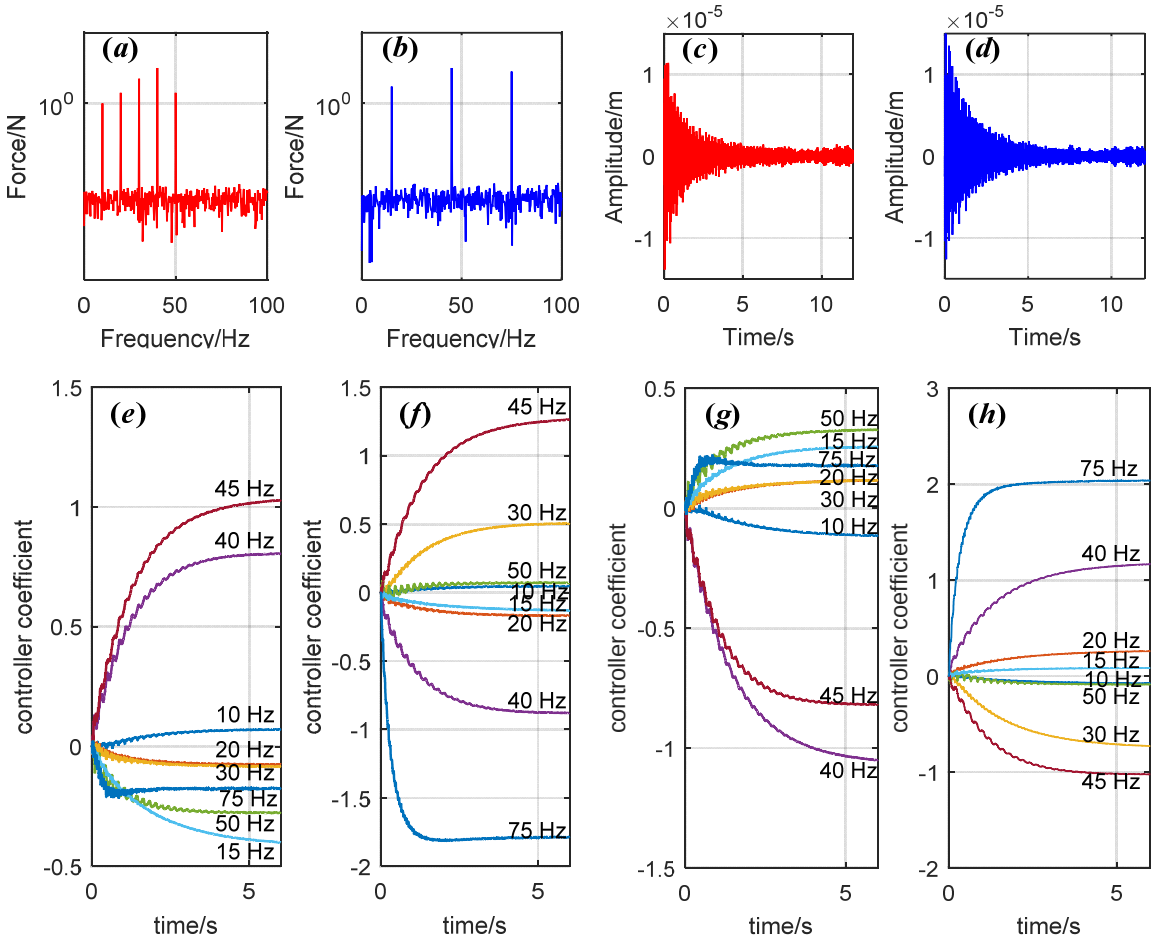


Figure 4: FEMilS case A, 2-source-2-input-2-output active vibration cancelation: (a) spectrum of primary force at P1; (b) spectrum of primary force at P2; (c) real-error signal at P3; (d) real-error signal at P4; (e) and (f) controller coefficient for the secondary source at P3; (g) and (h) controller coefficient for the secondary source at P4

### 5.3 Case B: 2-source-2-input-2-output active spectral reshaping

In case B, the layouts of primary sources, secondary sources and error sensors are the same as that in case A. The primary forces are the same as shown in Figure **4** (a) and (b), so the target frequency is $[10\ 15\ 20\ 30\ 40\ 45\ 50\ 75]^T$ Hz. The equalization parameters are different from case A. The equalization vector for P3 is $[1\ 0\ 0.4\ 0\ 1.5\ 0\ 0.4\ 0]^T$, so the target amplitude vector is $[1\ 0\ 2\ 0\ 3\ 0\ 4\ 0]^T \times 10^{-6}$m. The equalization vector for P4 is $[0\ 1.5\ 0\ 0.2\ 0\ 1.3\ 0.125]^T$, so the target amplitude vector is $[0\ 3\ 0\ 2\ 0\ 4\ 0\ 1]^T \times 10^{-6}$m. The sampling frequency is 2048Hz, the sampling time is 16s, and the step-size is $2\times10^{8}$. Figure **5** (a) and (b) shows the real error signal of P3 and P4. Figure **5** (c) and (d) shows the pseudo-error signal of P3 and P4. It can be seen that when the pseudo-error signal approach to zeroes, the real-error signal approach to a pre-defined signal. Figure **5** (e) and (f) shows the spectrum of real-error signal of P3 and P4, respectively, at 10s when the control is on and off. It can be seen that when the control is on, the residual spectrum are successfully reshaped according to the target, even though there are different targets at P3 and P4.

## 6. Conclusion

In this paper, we first introduced a universal MIMO narrowband FXLMS for multiple-frequency vibration control, i.e., MIMO-ANE algorithm, using matrix representation. Then, the convergence boundary of MIMO-ANE is derived in mean square sense. Afterwards, a finite element model in-

loop simulation (FEMilS) scheme is illustrated. The MIMO-ANE algorithm is verified on a variable section cylindrical structure based on FEMilS.

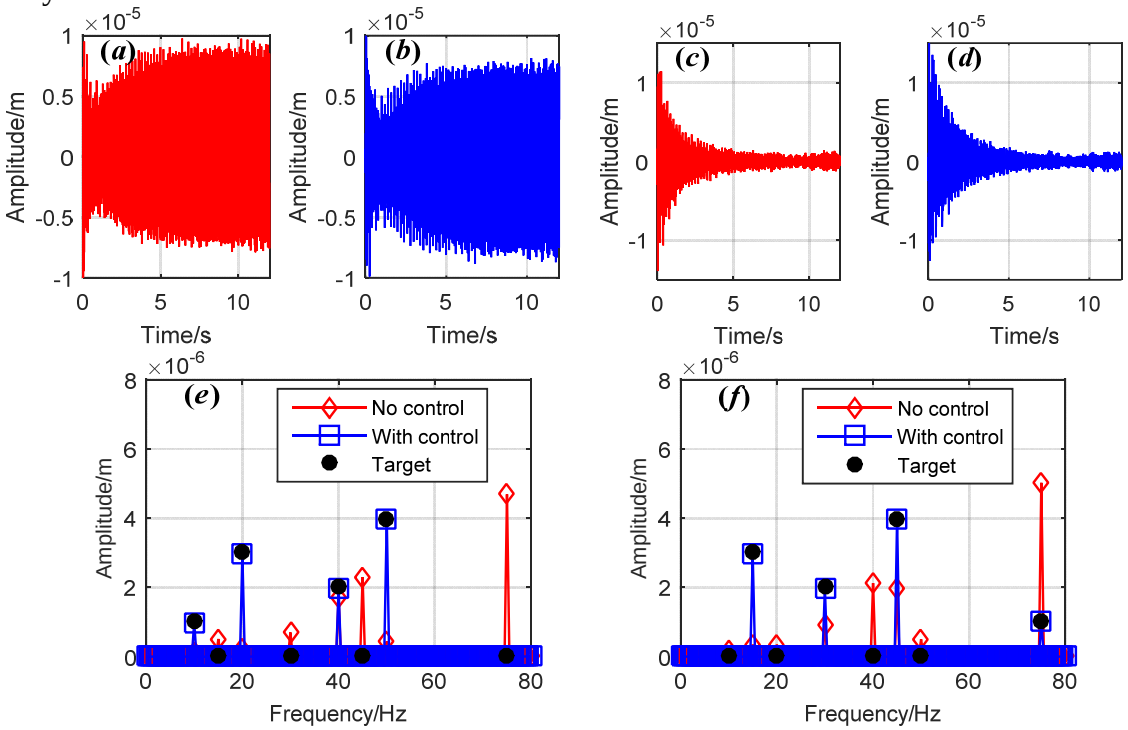


Figure 5: FEMilS case B, 2-source-2-input-2-output active spectral reshaping: (a) real-error signal at P3; (b) real-error signal at P4; (c) pseudo-error signal at P3; (d) pseudo-error signal at P4; (e) spectrum of the 10$^{th}$ second real-error signal at P3 when control is on and off; (f) spectrum of the 10$^{th}$ second real-error signal at P4 when control is on and off

## 7. Acknowledgments

This work is supported by National Natural Science Foundation of China (Nos. 51405370) and China Postdoctoral Science Foundation (Nos. 2016T90908, 2016M590937).

## REFERENCES

1 An, F.Y., Sun, H.L., Li, X.D., Adaptive Active Control of Periodic Vibration Using Maglev Actuators, *Journal of Sound and Vibration*, **331**(9), 1971-1984,(2012).
2 Liu, J., Chen, X., Gao, J., Zhang, X., Multiple-Source Multiple-Harmonic Active Vibration Control of Variable Section Cylindrical Structures: A Numerical Study, *Mechanical Systems and Signal Processing*, **81**(461-474,(2016).
3 Kuo, S.M., Morgan, D.R., Active Noise Control: A Tutorial Review, *Proceedings of IEEE*, **87**(6), 943-973,(1999).
4 Fuller, C.C., Elliott, S., Nelson, P.A., *Active Control of Vibration*, Academic Press, (1996).
5 Kuo, S.M., Morgan, D.R., *Active Noise Control Systems: Algorithms and DSP Implementations*, John Wiley & Sons, Inc, New York, (1996).
6 Kuo, S.M., Ji, M.J., Principle and Application of Adaptive Noise Equalizer, *IEEE Transactions On Circuits and Systems. II, Analog and Digital Signal Processing*, **41**(7), 471 - 474,(1994).
7 Liu, J., Chen, X., Adaptive Compensation of Misequalization in Narrowband Active Noise Equalizer Systems, *IEEE/ACM Transactions On Audio, Speech, and Language Processing*, **24**(12), 2390-2399,(2016).
8 Malgaca, L., Integration of Active Vibration Control Methods with Finite Element Models of Smart Laminated Composite Structures, *Composite Structures*, **92**(7), 1651-1663,(2010).
9 Khot, S.M., Yelve, N.P., Modeling and Response Analysis of Dynamic Systems by Using ANSYS (C) and MATLAB (C), *Journal of Vibration and Control*, **17**(6), 953-958,(2011).
10 Liu, J., Zhang, X., Chen, X., Modeling and Active Vibration Control of a Coupling System of Structure and Actuators, *Journal of Vibration and Control*, **22**(2), 382-395,(2016).